

## Electronic Supplementary Information

# Multiple Homogeneous Immunoassays Based on Quantum Dots-Gold Nanorods FRET Nanoplatform

Qinghui Zeng<sup>a</sup>, Youlin Zhang<sup>a</sup>, Xiaomin Liu<sup>a</sup>, Langping Tu<sup>a</sup>, Xianggui Kong<sup>\*a</sup> and Hong Zhang<sup>\*b</sup>

<sup>a</sup> State Key Laboratory of Luminescence and Applications, Changchun Institute of Optics, Fine Mechanics and Physics, Chinese Academy of Sciences, 3888 Eastern South Lake Road, Changchun 130033, China

<sup>b</sup> Van't Hoff Institute for Molecular Sciences, University of Amsterdam, Science Park 904, 1098 XH Amsterdam, The Netherlands

### Synthetic Procedures:

#### Chemicals.

Chloroauric acid trihydrate ( $\text{HAuCl}_4 \cdot 3\text{H}_2\text{O}$ ,  $\geq 99.9\%$ ), sodium borohydride ( $\text{NaBH}_4$ ,  $\geq 98\%$ ), 1-Ethyl-3-(3-dimethylaminopropyl) carbodiimide hydrochloride (EDC,  $\geq 99\%$ ), and sulfo-N-hydroxysulfosuccinimide (sulfo-NHS,  $\geq 98.5\%$ ) were purchased from Aldrich. Hexadecyltrimethylammonium bromide (CTAB,  $\sim 99\%$ ) and L-ascorbic acid ( $\geq 99.5\%$ ) were purchased from Sigma. Silver nitrate ( $\text{AgNO}_3$ ,  $\geq 99\%$ ) was purchased from Fluka. HBsAg, HBeAg, HBsAb1, HBsAb2, HBeAb1, HBeAb2 and BSA were obtained from H & R Bioscience Co., Ltd.. All the chemicals were used as received without further purification. Deionized water was purified through a Milli-Q water purification system and the resistivity was  $18.2 \text{ M}\Omega \cdot \text{cm}$

## Synthesis of gold nanorods with low aspect ratio

The synthesis of gold nanorods was a seed-mediated growth procedure, in which Au salt was reduced initially with a strong reducing agent, in water at room temperature, to produce about 4 nm seed particles. Simply, the Au seed particles were prepared by reduction of  $\text{HAuCl}_4$  (0.25 mM) in 0.1 M CTAB solution with the reduced reagent-ice-cold sodium borohydride (0.6 mM). Subsequent reduction of more metal salt with a weak reducing agent, in the presence of structure-directing additives, leads to the controlled formation of gold nanorods of specified aspect ratio. Briefly, a 25 mL growth solution was prepared by reduction of 0.5 mM  $\text{HAuCl}_4$  in a solution containing 0.1 M CTAB, 0.06 mM silver nitrate and 176  $\mu\text{L}$  of 0.08 M ascorbic acid. The color of the solution rapidly changed from golden to colorless after the introduction of ascorbic acid. 36  $\mu\text{L}$  of the seed solution was then added into the growth solution and the color of the solution slowly changed from colorless to deep purple. Ultimately, the bilayer CTAB-coated gold nanorods with plasmon absorption peaks at 509 (transverse plasmon band) and 776 nm (longitudinal plasmon band) were obtained after several hours' stirring. The schematic growth mechanism is shown in the up line of Scheme S1. As is shown in the FE-SEM of Fig. 1a, the size of the prepared nanorods is mainly 13 nm in width and 46 nm in length. According to the calculation from the absorption peaks<sup>[1]</sup> and FE-SEM result shown in Fig. 1, we can conclude that the aspect ratio of the original GNRs is  $\sim 3.5$ .

Scheme S1 illustrates the growth process of high aspect ratio and low aspect ratio GNRs, the low aspect ratio nanorods were prepared by the self-assembling approach of the originally seeded grown nanorods with high aspect ratio. Simply, the GNRs with aspect ratio 3.5 were kept storing at about 26 °C without any management for the self-assembly growth. The intended GNRs selected at different time intervals were centrifuged at 9600 rpm for more than 10 minutes to gently remove the excessive metal ions and CTAB molecules in the supernatant solution for terminating the self-assembly growth. As shown in Fig. 1, when the GNRs were kept undisturbed for 19 days, 29 days, and 36 (or even more than 36) days, the aspect ratio was gradually evolved from 3.5 to 2.9, 2.3, and ultimate 1.9, which evolution process can be proved well from both the variation of the FE-SEM results and absorption spectra. The ratio of the optical density between transverse plasmon band and longitudinal plasmon band were thus evolved from 1:7.0, to 1:4.8, 1:2.4 and 1:1.6. Because the high aspect ratio GNRs' plasmon resonance absorption is generally located as near-infrared region and the double plasmon absorption peaks are almost non-comparative, in other words, the optical density of the long-wavelength peak is greatly higher than the short-wavelength peak, which widely restrict the multiple immunoassays synchronously based on the FRET between a single GNR and multiple QDs, the final GNRs (aspect ratio=1.9) with plasmon absorption peaks at 520 and 629 nm were selected as the FRET acceptor for the HIA in our

work consequently. According to the method by Murphy et al.,<sup>[1]</sup> the concentration of the obtained GNRs was estimated to be about 3 nM for the next investigations.

### **Synthesis of aqueous CdTe/CdS core/shell quantum dots**

The 3-mercaptopropionic acid stabilized CdTe/CdS core/shell QDs were prepared according to our previous work.<sup>[2]</sup> The green and red CdTe/CdS core/shell QDs were emitted at 521 and 629 nm with QY of 60% and 40%, respectively. The average size of the aqueous CdTe/CdS core/shell QDs was calculated to be only 3 nm for GQDs and 6 nm for RQDs, which successfully discards the drawback of the large size (12–30 nm) water-soluble QDs after the multilayer coating, e.g., phospholipids, silica, or polymer, etc..<sup>[3-5]</sup> This is because the small dimension would dramatically improve the biological labeling and detection efficiency. Most important, the thinner surface capped layer will greatly increase the FRET efficiency when the QDs are applied as the energy transfer donors because FRET efficiency is inversely proportional to the sixth-power of the distance between donor and acceptor.

### **Conjugation of GNRs and antibody**

Because the short nanorods appear to be more chemically reactive than long nanorods.<sup>[6]</sup> It is thus easily controlled to prepare the GNRs-Ab conjugates with the non-covalent adsorption methods.<sup>[7,8]</sup> Basically, 60 pmol GNRs were mixed with 6 nmol antibodies for single label and separately equal amount of 3 nmol antibodies for multiple labels via a gentle stirring. In order to immobilize the HBsAb1 (for single HIA), HBeAb1 (for single HIA) and the equally proportional mixture of HBsAb1 and HBeAb1 (for multiple HIA) sufficiently, the adsorption time of Ab on GNRs should be enough (not less than 2 h). After the non-covalent adsorption, the GNRs-Ab conjugates were blocked by addition of 1% BSA solution and a gentle stirring afterwards. The resulting conjugates were collected by centrifugation of the samples at 9600 rpm for more than 10 minutes.

### **Conjugation of QDs and antibody**

The HBsAb2 and HBeAb2 were conjugated to the CdTe/CdS core/shell QDs with equal molar proportion classically by using EDC and sulfo-NHS as cross-linking reagent.<sup>[3,9]</sup> The schematic route of the covalent conjugation is shown in Scheme S2. The GQDs were coupled with HBsAb2 and the RQDs were coupled with HBeAb2. Firstly, 0.1 mL of QDs (60  $\mu$ M) was mixed with 10  $\mu$ L of EDC and sulfo-NHS in phosphate buffer saline (PBS, pH 7.4) with the molar ratio of 1:100:200. After 30 min of magnetic stirring, 6 nmol antibodies were added into the reacted bottle and stirred at room temperature for another 2 h. In this way, the amide linkage can be formed through the amino of the Ab and the active carboxyl of QDs. After this procedure, the QDs-Ab conjugates were blocked by addition of 1% BSA

solution and a gentle stirring afterwards. In order to remove the excess small molecules, e.g., EDC and sulfo-NHS, the resulting samples were centrifuged in Microcon Centrifugal Filter Devices (50,000 Nominal Molecule Weight Limit).

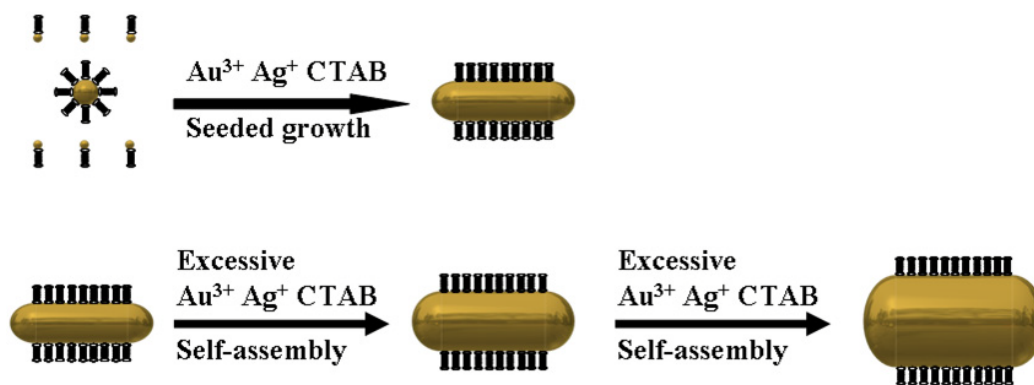
### **Homogeneous immune detection based on the FRET from QDs to GNRs**

Single HIA: as shown in Scheme 1, firstly, 30  $\mu\text{l}$  BSA blocked GNRs-Ab1 (0.18  $\mu\text{M}$ ) and QDs-Ab2 (0.18  $\mu\text{M}$ ) conjugates were mixed together in the PBS (pH 7.4) solution, the detected antigens with different content were then added into the solution for about one hour's Ag-Ab immune reactions to achieve different concentrations of 4.5, 9, 18, 36, 72, 144, 288, 576 and 1152 ng/ml for HBsAg and 4.2, 8.3, 16.5, 33, 66, 132, 264, 528 and 1056 ng/ml for HBeAg. The whole volume of the detected solutions was controlled as 300  $\mu\text{l}$ . The resultant mixtures were poured into a 2 mm path length quartz cell for additional PL measurements. The control experiments were also carried out where no antigen was added into the solutions. Because the FRET induced decay of QDs' fluorescence is relevant to the detected antigens, which can be calculated well by the subtraction value of the PL intensity of QDs compared with that of the control sample, we can thus get the immune detection curve readily.

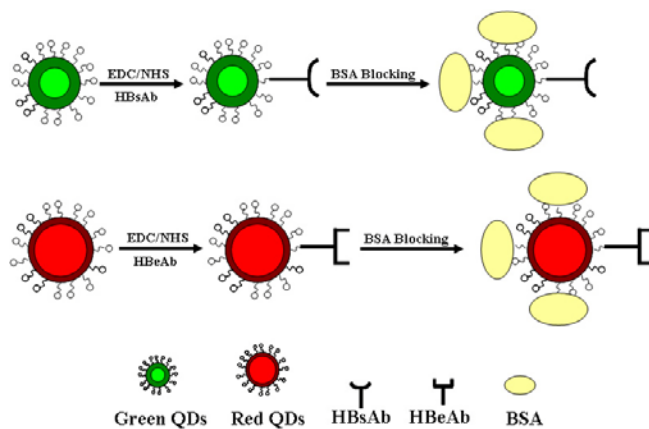
Multiple HIA: as shown in Scheme 1, firstly, 30  $\mu\text{l}$  BSA blocked GNRs-Ab1 (0.09  $\mu\text{M}$ ) and QDs-Ab2 (0.09  $\mu\text{M}$ ) conjugates were mixed together in the PBS (pH 7.4) solution, the detected antigens with different content were then added into the solution for about one hour's Ag-Ab immune reactions to achieve different concentrations of 4.5, 9, 18, 36, 72, 144, 288 and 576 ng/ml for HBsAg and 4.2, 8.3, 16.5, 33, 66, 132, 264 and 528 ng/ml for HBeAg. The whole volume of the detected solutions was controlled as 300  $\mu\text{l}$ . The resultant mixtures were poured into a 2 mm path length quartz cell for additional PL measurements. The control experiment was also carried out where no antigen was added into the solution. Because the FRET induced decay of QDs' fluorescence is relevant to the detected antigens, which can be calculated well by the subtraction value of the PL intensity of QDs compared with that of the control sample, we can thus get the immune detection curve readily.

### **Characterization:**

The size and morphology of GNRs were characterized by field emission scanning electron microscopy (FE-SEM, Hitachi, S-4800). Ultraviolet-visible (UV-vis) absorption and fluorescent emission spectra were measured at room temperature by a UV-3101 spectrophotometer and a Hitachi F-4500 fluorescence spectrofluorimeter, respectively. Unless mentioned otherwise, the excitation wavelength for PL spectra was set at 400 nm.



**Scheme S1** The schematic growth of high aspect ratio of gold nanorods and the evolution of self-assembly growth from high aspect ratio GNRs to low aspect ratio GNRs.



**Scheme S2** The schematic route of the covalent conjugation of QDs to HBsAb and RQDs to HBeAb by using EDC/NHS as the condensing agents.

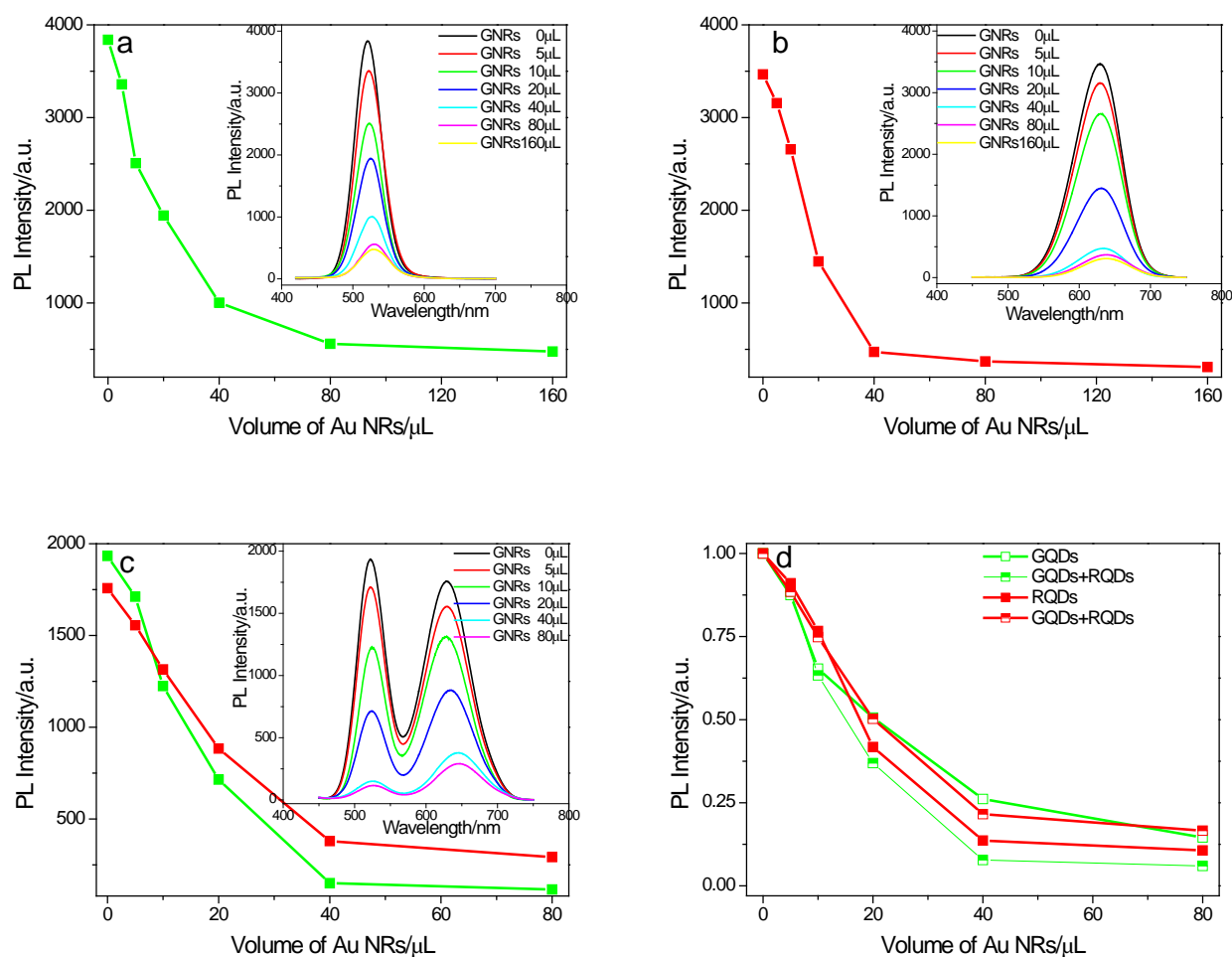
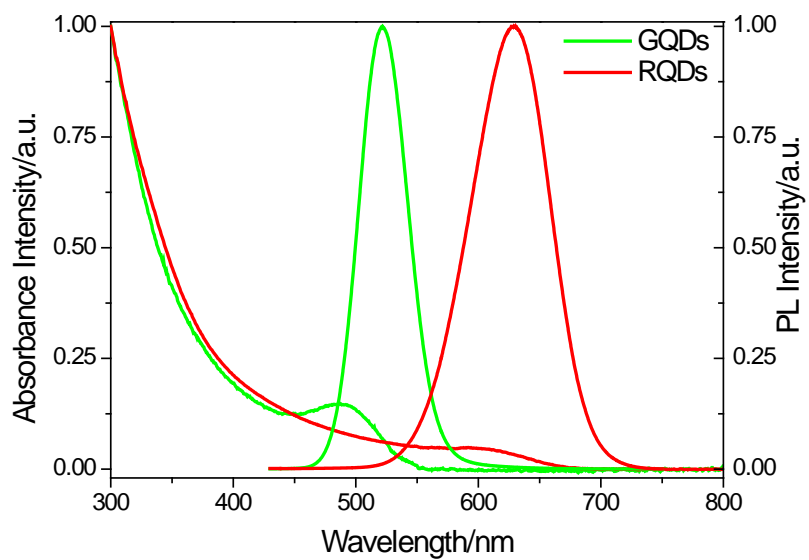


**Fig. S1** (a, b) The variation of the PL intensity at the GQDs (green square line in a) and RQDs (red square line in b) emission peaks after addition of different volumes of GNRs. The volume of GNRs was increased from 5 to 10, 20, 40, 80 and 160  $\mu\text{L}$ , and the concentration of GQDs and RQDs were kept constant as 12 nM. Inset is the relative PL spectra evolution of GQDs (a) and RQDs (b). (c) The variation of the PL intensity at the GQDs (green square line) and RQDs (red square line) emission peaks of the mixture of GQDs and RQDs after addition of different volumes of GNRs. The volume of GNRs was increased from 5 to 10, 20, 40 and 80  $\mu\text{L}$ , and the concentrations of GQDs and RQDs were kept constant as 6 nM. Inset is the relative PL spectra evolution of the mixed double color QDs. (d) The variation of the normalized PL intensity at the GQDs (green square line, shown in a and c) and RQDs (red square line, shown in b and c) emission peaks after addition of different volumes of GNRs.

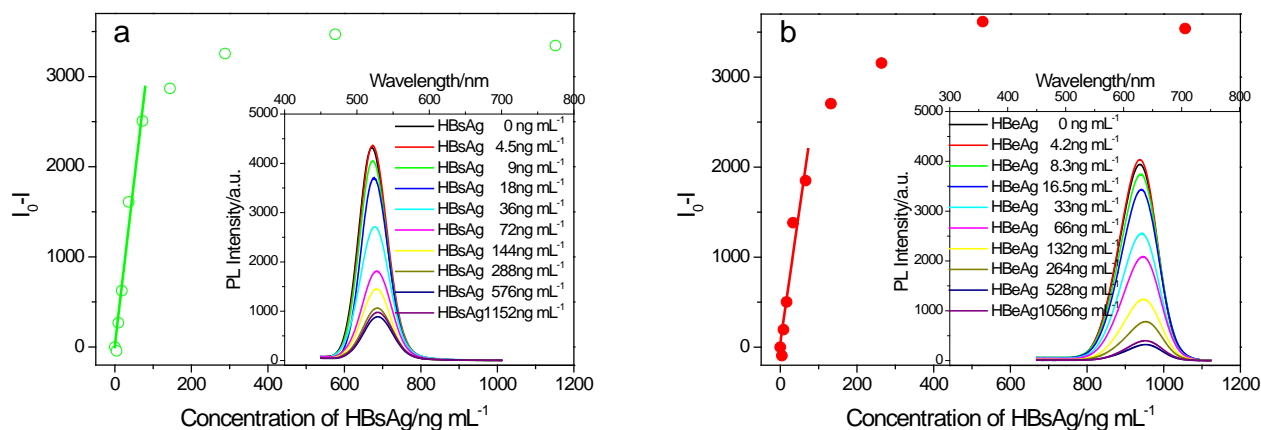
The FRET efficiency can be estimated by  $\Phi_{\text{FRET}} = 1 - I_{\text{DA}}/I_{\text{D}}$  assuming that other quenching mechanisms, such as re-absorption, are negligible,<sup>10</sup> where  $I_{\text{DA}}$  and  $I_{\text{D}}$  are the fluorescence intensities of the donor with and without the presence of the acceptor, respectively. From the PL spectra shown in Fig. S1a and Fig. S1b, the FRET efficiency could achieve 87.6% for GQDs and 91.1% for RQDs as the volume of GNRs reaches the saturated value. Such high FRET efficiencies were attributed to a combination of factors, as considering the characteristics of the present design and the rule of FRET efficiency. Firstly,

GNRs have larger surface area and lower curvature, which can increase the quenching sites and improve the quenching efficiency. Secondly, GNRs have a large extinction coefficient. As are reported previously,<sup>1,11</sup> the extinction coefficient of GNRs is more than  $10^9 \text{ M}^{-1}\text{cm}^{-1}$ , which is about 4-5 orders of magnitude higher than that of fluorescent dyes. Thirdly, the spectra of the GNRs and QDs overlap perfectly because of the high tunability of the spectra of our tailor-designed QDs donors and GNRs acceptors. Obviously, the more the spectra overlap between donor and acceptor is, the greater the energy transfer efficiency of a FRET system will be.

It is worth noting that the FRET efficiency of GQDs is slightly increased to 94.0% and the FRET efficiency of RQDs is slightly decreased to 83.4% when both GQDs and RQDs are mixed together with the GNRs compared to the single color QDs' final FRET efficiencies. As shown in Fig. S1d, there is a little PL recovery of RQDs and a further PL decay of GQDs for the equally proportional mixing of GQDs and RQDs when the volume of GNRs was surpassed 10  $\mu\text{L}$ , which may be due to the unavoidable FRET process from the GQDs to RQDs themselves when the amount of green and red QDs onto the GNRs surface are big enough to show the slight self FRET signal.<sup>[12]</sup> The spectral overlap to show the probable FRET mechanism from GQDs to RQDs is shown in Fig. S2.



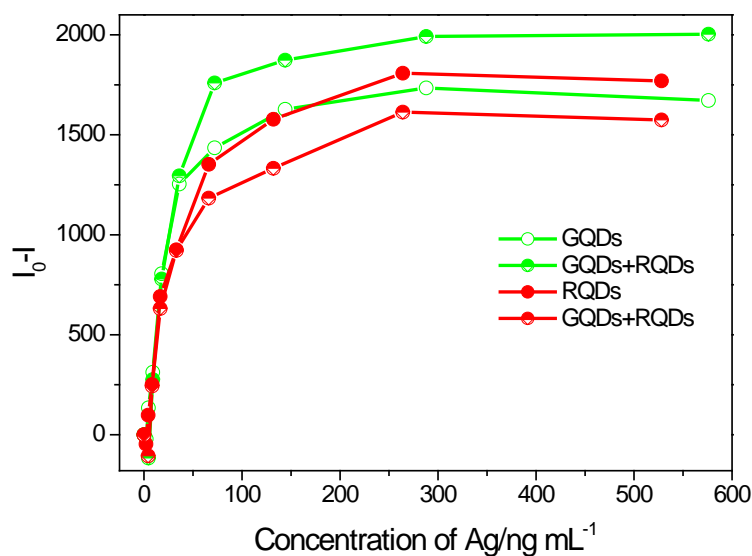
**Fig. S2** Normalized absorption and PL spectra of green (green line) and red (red line) QDs.



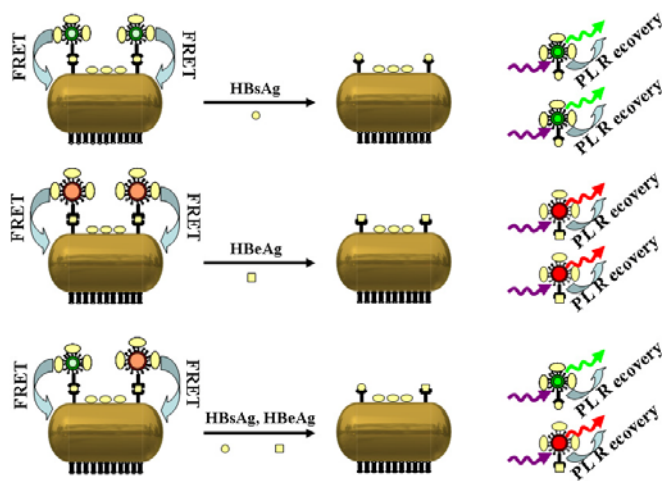
**Fig. S3** FRET-based single detection of antigens. The relationship between the subtracted PL intensity ( $I_0 - I$ ) of GQDs-HBsAb2 (a) and RQDs-HBeAb2 (b) in the presence of GNRs-HBsAb1 (a), GNRs-HBeAb1 (b), and the detected HBsAg (a), HBeAg (b) with different concentrations. Inset is the relative PL spectra variation of the GQDs (a) and RQDs (b). The excitation wavelength is 400 nm.

Fig. S3a (or Fig. S3b) shows the experimental results where the PL intensity from bound GQDs-HBsAb (or RQDs-HBeAb) conjugate was measured over a concentration range of HBsAg (or HBeAg) till 1152  $\text{ng mL}^{-1}$  (or 1056  $\text{ng mL}^{-1}$ ). It should be noted that the signal increased monotonically with the increase of the concentration of HBsAg until 576  $\text{ng mL}^{-1}$  for single immunoassays. At the same time, the signal increases monotonically with the increase of the concentration of HBeAg until the value reached 528  $\text{ng mL}^{-1}$  for single immunoassays. Hereby, the detection range of HBsAg (or HBeAg) can achieve 576 (or 528)  $\text{ng mL}^{-1}$  for the single immunoassays. The linear calibration curve could be obtained as  $Y = 28.455 + 36.07X$  ( $9 \leq X \leq 72$   $\text{ng mL}^{-1}$ , correlation coefficient  $R = 0.988$ ) for single HBsAg detection by using GQDs as FRET donor,  $Y = 55.098 + 29.52X$  ( $8.3 \leq X \leq 66$   $\text{ng mL}^{-1}$ ,  $R = 0.967$ ) for single HBeAg detection by using RQDs as donor. The LOD of HBsAg and HBeAg single immune detection is 9.0 and 8.3  $\text{ng mL}^{-1}$ , respectively.

After calculating the FRET efficiency, we find that the maximum FRET efficiencies of GQDs-GNRs and RQDs-GNRs have decreased from 87.6% and 91.1% to 77.4% and 89.9% respectively before and after the configuration of the sandwich structure. This may be due to the fact that the distance between QDs and GNRs would be larger due to the intermediate layers of antibodies and antigens.



**Fig. S4** FRET-based single and multiple detections of antigens. The relationship between the subtracted PL intensity ( $I_0 - I$ ) of GQDs-HBsAb2, RQDs-HBeAb2 and the mixture of GQDs-HBsAb2 and RQDs-HBeAb2 in the presence of GNRs-HBsAb1, GNRs-HBeAb1 and the mixture of GNRs-HBsAb1 and GNRs-HBeAb1, and the detected HBsAg, HBeAg and the mixture of HBsAg and HBeAg with different concentrations. The relative PL spectra variation of the GQDs, RQDs and the mixture of GQDs and RQDs are shown in Fig. S3 and Fig. 3.



**Scheme S3** The schematic PL recovery mechanism induced by the supersaturated detection antigens.

Theoretically, when the amount of the detected antigens surpasses the saturated amount of the labeled antibodies, e.g.,  $1152 \text{ ng mL}^{-1}$  for HBsAg (or  $1056 \text{ ng mL}^{-1}$  for HBeAg) in single immunoassays and  $576 \text{ ng mL}^{-1}$  for HBsAg (or  $528 \text{ ng mL}^{-1}$  for HBeAg) in multiple immunoassays, there should be a flat response for the immune detection. Actually, there was a slight decrease in the detection curve, which is due to the fact that addition of HBsAg or HBeAg to the solution displaced the sandwich antigens and resulted in a PL recovery of the QDs (Scheme S3).

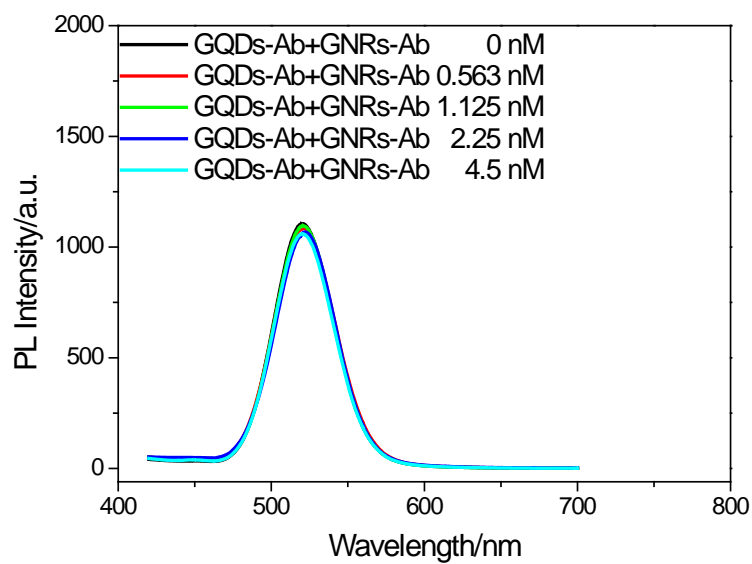


**Fig. S5** The PL spectra variation of GQDs-Ab when the concentration of GNRs-Ab was increased from 0.563 to 4.5 nM. The concentration of GQDs was kept constant at 4.5 nM. The excitation wavelength was 400 nm.

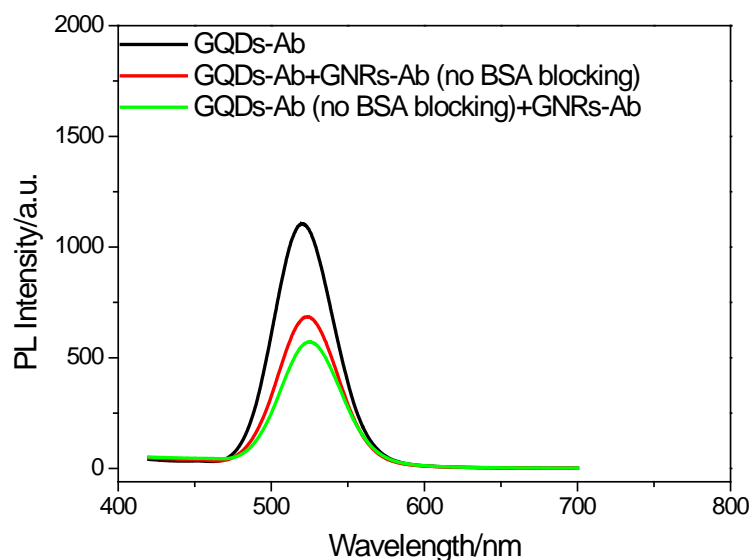


**Fig. S6** The PL for the QDs-Ab and GNRs-Ab solutions, no matter GNRs-Ab conjugates (red line) or QDs-Ab conjugates (green line) were constructed without the BSA blocking procedure, the PL intensity will decrease obviously. The concentration of GQDs was kept constant at 4.5 nM. The excitation wavelength was 400 nm.

To further demonstrate the high specificity of the FRET based HIA, we also performed some non-specific detection. It is well known that the BSA blocking is essential for the homogeneous immune detection, which can be proved by the change of the PL spectra when the QDs-Ab and GNRs-Ab are mixed together. In the present case, we have proved that it is vital to block both the QDs-Ab and the GNRs-Ab conjugates with common proteins such as BSA molecules to drastically reduce the impact of the non-specific adsorption to the HIA. As shown in Fig. S6, no matter GNRs-Ab conjugates (red line) or QDs-Ab conjugates (green line) were constructed without the BSA blocking procedure, the non-specific adsorption induced FRET would happen spontaneously and led to an obvious PL decay. Based on the changeless PL spectra shown in Fig. S5 where the different concentration BSA blocked GNRs-Ab conjugates were mixed with the BSA blocked QDs-Ab solutions, we can conclude that both the QDs-Ab conjugates and GNRs-Ab conjugates were blocked with 1% BSA solutions successfully to achieve the FRET based homogeneous immune detection favourably. To sum up, it can be concluded that our multiple homogeneous immune detections based on the FRET process from QDs to GNRs were feasible and conceivable.

## Notes and references

- 1 C. J. Orendorff and C. J. Murphy, *J. Phys. Chem. B* 2006, **110**, 3990–3994.
- 2 Q. Zeng, X. Kong, Y. Sun, Y. Zhang, L. Tu, J. Zhao and H. Zhang, *J. Phys. Chem. C* 2008, **112**, 8587–8593.
- 3 Q. Zeng, Y. Zhang, K. Song, X. Kong, M. C. G. Aalders and H. Zhang, *Talanta* 2009, **80**, 307–312.
- 4 W. C. Law, K. T. Yong, I. Roy, H. Ding, R. Hu, W. W. Zhao and P. N. Prasad, *Small* 2009, **5**, 1302–1310.
- 5 K. T. Yong, W. C. Law, I. Roy, Z. Jing, H. J. Huang and M. T. Swihart, *J. Biophotonics* 2011, **4**, 9–20.
- 6 C. J. Murphy, T. K. Sau, A. M. Gole, C. J. Orendorff, J. X. Gao, L. F. Gou, S. E. Hunyadi and T. Li, *J. Phys. Chem. B* 2005, **109**, 13857–13870.
- 7 X. H. Wang, Y. Li, H. F. Wang, Q. X. Fu, J. C. Peng, Y. L. Wang, J. Du, Y. Zhou and L. S. Zhan, *Biosens. Bioelectron.* 2010, **26**, 404–410.
- 8 Y. Qiu, Y. Liu, L. M. Wang, L. G. Xu, R. Bai, Y. L. Ji, X. C. Wu, Y. L. Zhao, Y. F. Li and C. Y. Chen, *Biomaterials* 2010, **31**, 7606–7619.
- 9 Y. Liu, R. Brandon, M. Cate, X. Peng, R. Stony and M. Johnson, *Anal. Chem.* 2007, **79**, 8796–8802.
- 10 Y. Xia, L. Song and C. Zhu, *Anal. Chem.* 2011, **83**, 1401–1407.
- 11 B. Nikoobakht, J. Wang and M. A. El-Sayed, *Chem. Phys. Lett.* 2002, **366**, 17–23.
- 12 S. A. Crooker, J. A. Hollingsworth, S. Tretiak and V. I. Klimov, *Phys. Rev. Lett.* 2002, **89**, 186802.